Communication

Dual-Linear Polarized Phased Array With 9:1 Bandwidth and 60° Scanning Off Broadside

Jingni Zhong, Alexander Johnson, Elias A. Alwan, and John L. Volakis

***Abstract*— We present, for the first time, a novel dual-linear polarized tightly coupled dipole array with integrated balun operating across a 9:1 bandwidth, from 2 to 18 GHz. This dual-linear polarized array employs a tightly coupled dipole topology and scans down to 60° from boresight. The overall geometry consists of cross-located tightly coupled dipoles integrated with a folded Marchand balun that serves as an impedance transformer to achieve a wideband feeding network. Notably, the traditional dielectric superstrate is replaced with double layers of frequency selective surfaces to enable scanning down to 60° in both E-, H-, and diagonal (D)-planes across the entire band. The design achieves VSWR < 3 across 2–18 GHz at broadside. This dual-polarized array is also demonstrated to have a good polarization isolation of −20 dB for most of the band. The array's total height is less than 12 mm (λ_{low}/10). The design is validated through fabrication and testing of an 11 × 11 prototype. The measurements of this prototype are presented and are in good agreement with simulations.**

***Index Terms*— Low-profile array, tightly coupled dipole array (TCDA), ultrawideband (UWB), wide-angle scanning.**

I. Introduction

Future wireless communication systems are expected to require much larger bandwidth to accommodate data growth and accommodate user demands. To cover the multiple frequency bands and/or scanning range, future mobile communication systems are expected to have multiple antennas. A single ultra-wideband (UWB) antenna can alleviate the need for multiple antennas. Examples include space-borne applications that may require a single UWB array to cover *S* (2–4 GHz), *C* (4–8 GHz), *X* (8–12 GHz), and *Ku* (12–18 GHz). In addition, as modern platforms are becoming smaller in size, there is a strong desire for inconspicuous integration on platforms such as small satellites, unmanned aerial vehicles, and automobiles, among others. Apart from being conformal, the proposed tightly coupled dipole arrays (TCDAs) are low profile and can provide improved directionality and cross polarization while scanning [1], [2].

Designs of the UWB phased arrays are often hindered by the size-bandwidth-scanning angle metric. For example, Vivaldi arrays or tapered slot arrays are known for their large operational bandwidth [3], [4], viz., 12:1 impedance bandwidth. However, Vivaldis are associated with large height up to $4 \times \lambda_{\text{high}}$, where λ_{high} is the wavelength at the highest operational frequency. This is because their overall bandwidth is associated with their length-to-width ratio [3].

As an alternative to Vivaldis, connected arrays were considered in the early 2000s [6], [7]. These arrays delivered up to about 4:1 bandwidth. To achieve larger bandwidth, the tightly coupled array (TCA) was introduced in [8]–[16]. Both the connected arrays and TCAs are of low profile with large operational bandwidth. It is worth mentioning that the latest design of Vivaldi array [5], also known as balanced antipodal Vivaldi antenna (BAVA), exhibits compact profile as low as $\lambda_{\text{high}}/2$ with a decade bandwidth. BAVAs achieve large bandwidth also by applying capacitive coupling between elements, through the U-channel structure. However, they are limited to 45° scanning.

A key aspect of TCDA is their integration with a wide bandwidth balun (TCDA-IB) [9]–[16]. Specifically, TCDAs are integrated with a folded Marchand balun [9] which serves as balanced feeding and as an impedance matching network. Nearly 7:1 bandwidth has been demonstrated by previous TCDAs. Furthermore, when a resistive card (R-card) is inserted into the substrate, the bandwidth of TCDA can be doubled to 13:1 [10], [11]. The R-cards mitigate ground plane reflections to extend the bandwidth. However, since R-cards lead to lower efficiency, they are not favored in this design. Besides their large bandwidth and low profile, TCDAs are also associated with a wide scanning angle. Previous designs demonstrated at least 45° scanning using dielectric slab loading. In [13], the dielectric slab is replaced with a frequency selective surface (FSS) structure. The latter is conveniently printed on the same substrate as the antenna and balun, substantially lower fabrication cost. Notably, the FSS structure extends TCDA's scanning to as much as 70° from broadside.

In this communication, we present a new version of TCDA that exhibits a larger bandwidth. This design is based on previous works in [15] and [16] but has the added features of larger bandwidth without using R-cards and includes a double layer FSS for improved wideband scanning performance in the E- and H-planes. The presented array is dual polarized and operates from 2 to 18 GHz with VSWR < 3. We also adapted the FSS superstrate to enable scanning down to 60° in the E-, H-, and diagonal (D)-planes with VSWR < 4 under most cases. This design also exhibits great polarization isolation of at least 20 dB. An 11 × 11 element prototype was fabricated and measured to verify the performance of our design. In summary, the design presented in this communication provides a practical solution toward the realization of 2–18 GHz wideband and wide-angle scanning phased array.

This communication is organized as follows. Section II describes the structure and design procedure of the TCDA leading to full-wave simulation. Section III presents the fabrication, assembly, and measurement of an 11 × 11 prototype. Section IV compares the features of this array with previous TCDAs. In Section V, we briefly discuss the challenges as relates to digital beamforming back-ends to enable UWB transceivers, together with our overall conclusions.

II. Array Design and Simulation

The proposed dual-linear polarized TCDA with integrated Marchand balun is depicted in Fig. 1. This model was created and analyzed as a periodically repeated unit cell using the commercial software High Frequency Structure Simulator (HFSS) of ANSYS.

Manuscript received May 19, 2018; revised November 30, 2018; accepted December 8, 2018. Date of publication January 10, 2019; date of current version March 5, 2019. *(Corresponding author: Jingni Zhong.)*

The authors are with the Department of Electrical and Computer Engineering, College of Engineering and Computing, Florida International University, Miami, FL 33174 USA (e-mail: jizhong@fiu.edu; ajohn326@fiu.edu; ealwan@fiu.edu; jvolakis@fiu.edu).

Color versions of one or more of the figures in this communication are available online at http://ieeexplore.ieee.org.

Digital Object Identifier 10.1109/TAP.2019.2891607

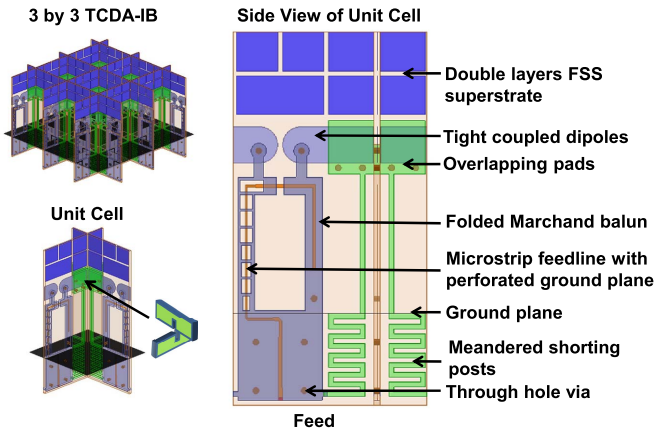

Fig. 1. Proposed dual-linear polarized TCDA-IB: example of a 3 × 3 array, periodic unit cell, and side view of the periodic unit cell.

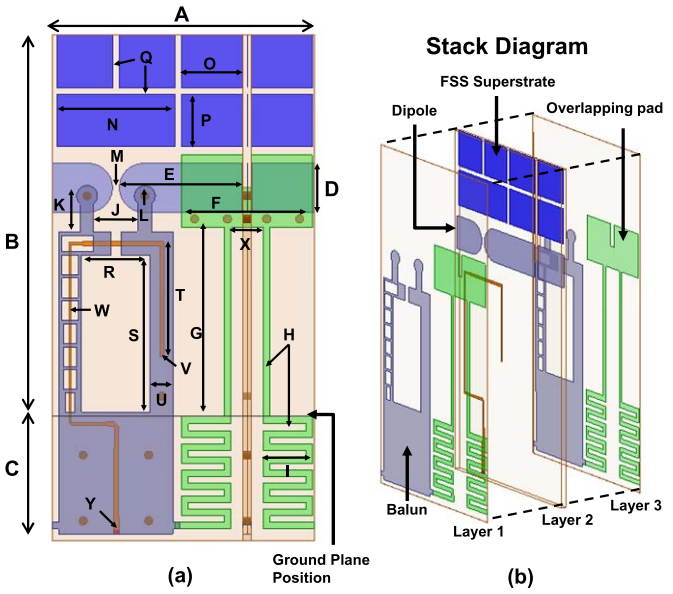

Fig. 2. Illustration of the proposed TCDA-IB periodic unit cell. (a) Design parameters noted from "A" to "Y." (b) Stack diagram.

The unit cell is composed of the following sections (from top to bottom): double-layer FSS superstrate, tightly coupled dipoles and overlapping pads, folded Marchand balun, microstrip feedline with perforated ground plane, meandered shorting posts, and ground plane. Detailed explanations on the functionalities of these components are provided in Sections II-A–D. The key design parameters and antenna stack diagram of the periodic unit cell are shown in Fig. 2. The final design values for the geometrical parameters are provided in Table I. As seen in Fig. 2, the proposed TCDA with integrated balun consists of three metal layers, hosted by two Rogers DiClad 880 substrates of 5 mil thickness each. The folded Marchand balun, overlapping pads, and meandered shoring post are placed on the first and third layers, connected by through-hole vias. Dual-layer FSS and tightly coupled dipoles are placed in the middle layer, together with the tapered feedline. The tapered feedline is sandwiched between two pieces of folded Marchand balun. The latter is used as the ground plane and together constitutes a microstrip feeding structure.

We provide design guidelines for the proposed dual-polarized TCDA-IB as follows.

TABLE I
OPTIMIZED DESIGN PARAMETERS SHOWN IN FIG. 2

Parameter	Value (mm)	Parameter	Value (mm)	Parameter	Value (mm)
A	8	J	1.36	S	4.8
B	11.6	K	1.35	T	3.5
C	3.7	L	0.4	U	0.7
D	1.5	M	0.2	V	0.12
E	3.75	N	3.6	W	0.08
F	3.8	O	1.87	X	1.01
G	5.95	P	1.6	Y	0.16
H	0.2	Q	0.2		
I	1.5	R	2.1		

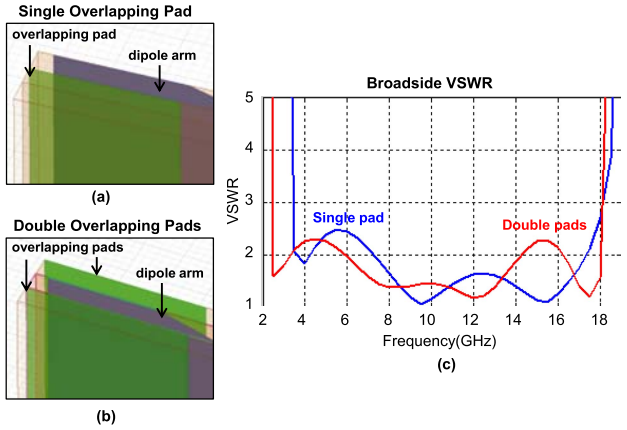

Fig. 3. Illustration of TCDA overlapping pads. (a) Single overlapping pad. (b) Double overlapping pads. (c) Simulated broadside VSWR.

A. Tightly Coupled Dipoles With Overlapping Pads

The dimensions of the dipole elements are carefully designed so that the distance between adjacent elements is kept less than $\lambda_{high}/2$ to avoid grating lobes. In previous TCDA designs [10]–[12], capacitive coupling between adjacent elements was realized by overlapping the dipole arms or by adding metal pads on another layer of the substrate in-between the dipoles [similar to that in Fig. 3(a)]. In this design, to achieve wider bandwidth, we placed the overlapping pads in-between the adjacent dipoles and on both sides of the dipole to increase coupling. Specifically, the overlapping pads are printed on the first and third layers and are connected in parallel by vias to double the capacitive coupling. Fig. 3 demonstrates a VSWR comparison of the TCDA using the single and double overlapping pads. The simulated broadside VSWR is shown in Fig. 3(c). As shown, double overlapping pads introduce a stronger capacitive coupling among the dipole elements to effectively extend the operational bandwidth.

B. Folded Marchand Balun and Microstrip Feedline

The folded Marchand balun is designed to provide a balanced feed to the dipole elements and serves as an impedance transformer. The balun is printed on layer 1 and layer 3, with the feedline sandwiched in-between. This feedline uses folded Marchand balun as its ground plane. A tapering of the feedline is also applied to transform the 50 Ω input port to the 150 Ω impedance at the dipole feed. The impedance change is achieved in two steps. For the first part (beneath the ground plane), we employed a linear

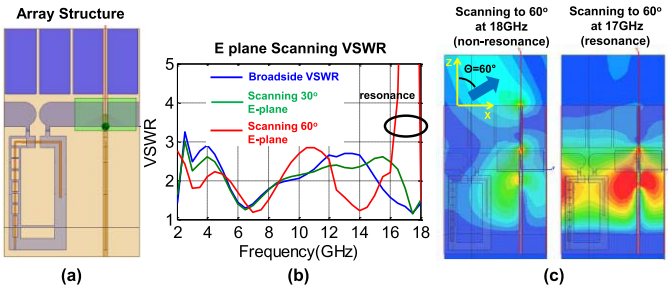

Fig. 4. Preliminary TCDA-IB design in [16] without meandered shorting posts. (a) Single array element. (b) Simulated VSWR when scanning in E-plane. (c) Simulated E-field distribution at the resonant frequency.

tapered microstrip width. For the second part (above the ground plane), we introduced perforations to the ground plane (similar to [13]). These perforations serve to further increase the characteristic impedance to reach 150 Ω.

C. Double-Layer FSS Superstrate

As described earlier, dielectric superstrates are commonly used to improve scanning. However, these dielectric slabs are heavy, add complexity to the assembly process, and can also cause trapped waves in the substrate at low scanning angles. To avoid these issues, we expanded upon the design in [13] by employing a double-layer FSS formed by metallic squares. These periodically repeated metallic squares replace the usual dielectric slab superstrate, implying much smaller weight, simpler fabrication/assembly, and wider angular scanning. Parametric studies suggest that the width and height of FSS strips (see Fig. 2) determine the operational frequency. Wider and taller FSS layers correspond to better matching to the TCDA-IB at low frequencies and vice versa. For our double-layer FSS, each layer is designed to contain metallic squares of small width and height. This is done to ensure good performance at the higher end of the band. At low frequencies, since the wavelength becomes significantly longer, the closely placed two-layer FSS behaves more such as a single FSS. That is, the smaller FSS patches are grouped with the near ones to represent larger FSS elements and therefore accommodate the low-frequency performance. Notably, the FSS structure is optimized with the rest of the array to achieve the best performance.

D. Meandered Shorting Posts

In [15] and [16], we presented a preliminary design of this UWB TCDA-IB. However, the design suffers from high-frequency resonance at 17 GHz while scanning in the E- and D-planes down to 60°. This behavior significantly reduces the available bandwidth while scanning as depicted in Fig. 4. To identify the cause of the mismatch at 17 GHz, we examined the fields within the unit cell. As seen in Fig. 4(c), the cause of the mismatch is due to a strong resonance. Notably, such resonances have been observed before in coupled array designs [14]. To circumvent the issue, the meandered shorting posts are added between the overlapping pads and the ground plane to disturb the resonance conditions. As shown in Fig. 5, a resonance-free impedance bandwidth from 2 to 18 GHz is now observed at broadside and while scanning down to 60°.

Fig. 5 presents the simulated VSWR of the proposed TCDA while scanning into E-, H-, and D-planes. As depicted at the bottom right of Fig. 5, the H-plane is associated with $\varphi = 0°$ cut, the E-plane corresponds to the $\varphi = 90°$ cut, and the D-plane refers to the $\varphi = 45°$ cut.

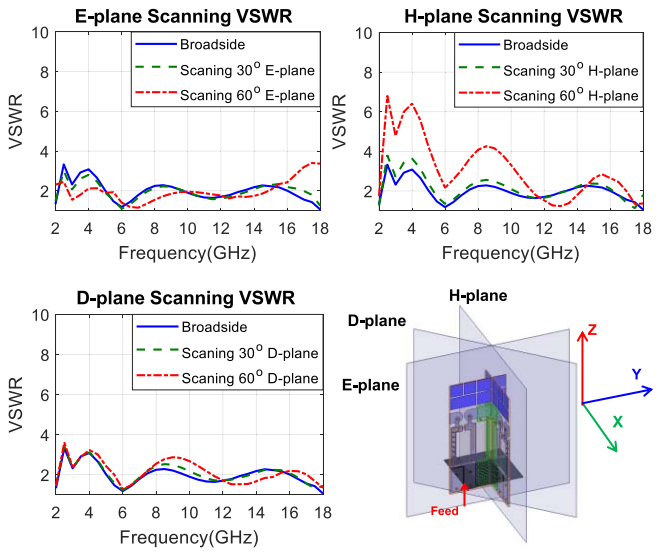

Fig. 5. Simulated VSWR of the proposed dual-linear polarized TCDA-IB while scanning into the E-, H-, and D-planes.

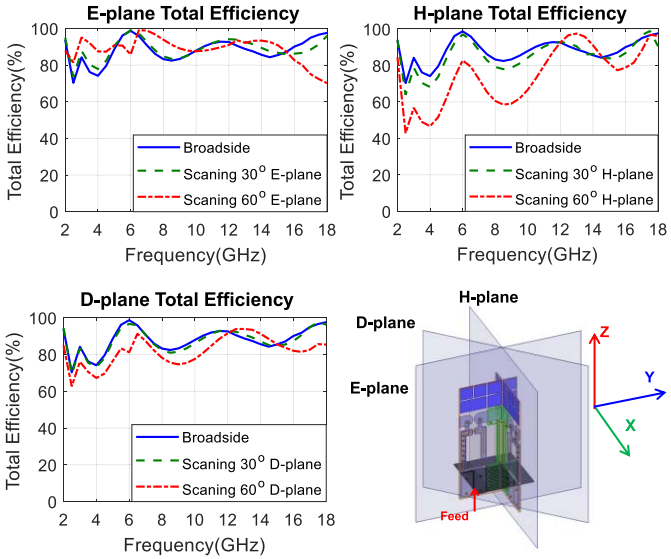

Fig. 6. Simulated total efficiency of the proposed dual-linear polarized TCDA-IB while scanning into the E-, H-, and D-planes.

As seen in Fig. 5, the dual-linear polarized TCDA operates from 2 to 18 GHz (9:1 bandwidth) with VSWR < 3 at broadside, and VSWR < 4 when scanning down to 60° in E- and D-planes and down to 30° while scanning into H-plane. The VSWR can increase up to VSWR $= 4$ when scanning to 60° in the H-plane across 5–18 GHz and even to VSWR $= 6$ at 2.5 to 4 GHz, also in the H-plane. Importantly, at the lower band, the tested 11×11 finite array has a dipolelike pattern and does not therefore have a distinct scanning beam. The efficiency of the designed array for both broadside and scanning cases are presented in Fig. 6. The averaged efficiency was computed to be ~85% while taking into account mismatch losses.

III. Prototype Fabrication and Measurement

The developed 9:1 TCDA design is validated by fabricating an 11×11 prototype, depicted in Fig. 7. This dual-polarized TCDA

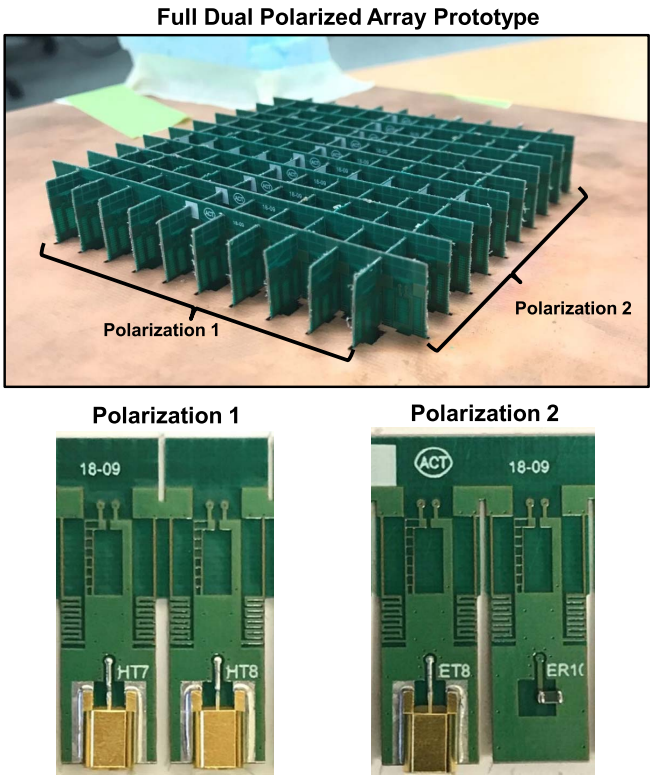

Fig. 7. Fabricated 11 × 11 UWB dual-linear polarized TCDA prototype and detailed illustration for elements in polarization 1 and 2.

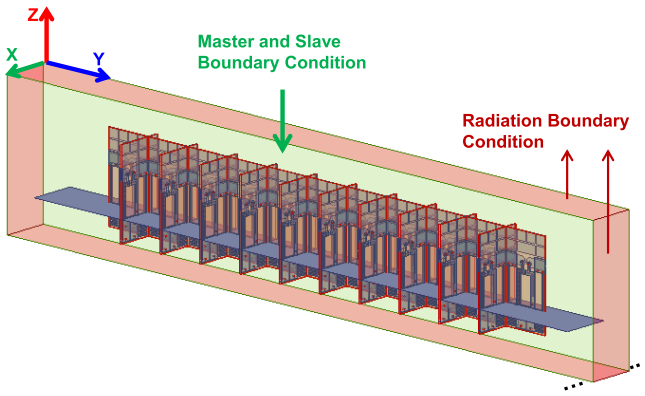

Fig. 8. Model setup for the semifinite TCDA-IB simulation.

prototype consists of 10 vertical and parallel printed circuit boards (PCBs) for each polarization of the planes. Each card contains 11 tightly coupled dipole elements (unit cells). Each unit cell elements are either fed via a 50 Ω subminiature push-on connectors or directly terminated by 50 Ω termination resistors. The 10 × 10 cards are assembled as in Fig. 7 (top) and placed on a 9″ × 11″ copper-clad laminated FR4 board to serve as a ground plane. The ground plane contains a set of laser-cut slots for securing the PCB cards.

To assess the radiation pattern and gain of our TCDA, we simulated a semifinite array as in Fig. 8. This simulation model includes 11 array elements lying in the y-direction. Along the x-direction, there are infinite elements.

The measured VSWR of center elements for the fabricated prototype is provided in Fig. 9 and compared with the same VSWR for the semifinite array simulation. As seen, measurements are in good

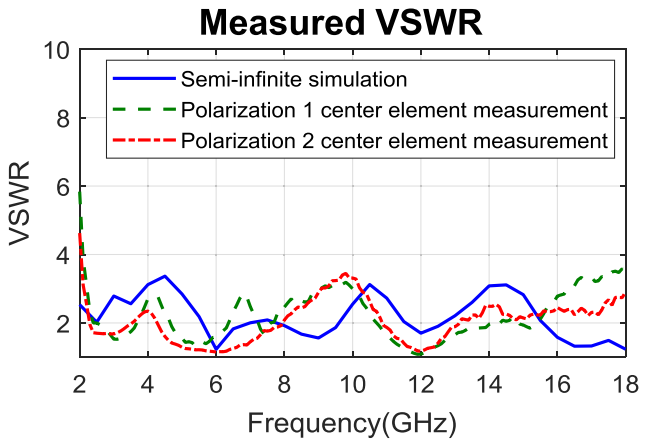

Fig. 9. Measured and simulated VSWR of center element.

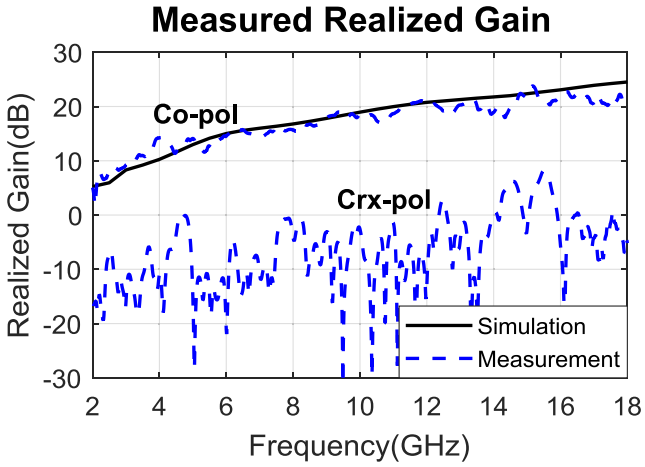

Fig. 10. Measured broadside co-polarized and cross-polarized realized gain, comparing with analytical data from the semifinite model.

agreement with simulations. Our measurements also verify that the array performances for both polarizations are almost identical. This is expected due to symmetry. The measured prototype also exhibits VSWR < 3 impedance bandwidth from 2.1 to 18 GHz, as shown in Fig. 9, again, verifying our design.

The realized gain and radiation pattern measurements were conducted following the unit excitation active element pattern method proposed in [17]. Using this method, the individual element pattern and gain are measured with all other elements terminated with a 50 Ω load. The overall simulated and measured realized gain for the co-polarization and cross-polarization patterns are given in Fig. 10. We note that the cross-polarization gain is defined following Ludwig's third definition [18]. As seen, the measured realized gain agrees well with simulations. Notably, the simulated cross-pol isolation is at about 40 dB [16], whereas the measured cross-pol isolation is around 20 dB. This is primarily due to the max isolation of the feeding horn (COBHAM H-1498).

Simulated and measured normalized radiation patterns in both E- and H-planes are provided in Figs. 11. and 12, respectively. The patterns are measured at 2.5, 8, 12, and 18 GHz with scanning down to 60°. Measurement and simulation fit very well in all cases. Note that since we do not have a 1–11 power splitter covering from 2 to 18 GHz, the radiation pattern was calculated from single element pattern multiplied with array factor with phase progression considered.

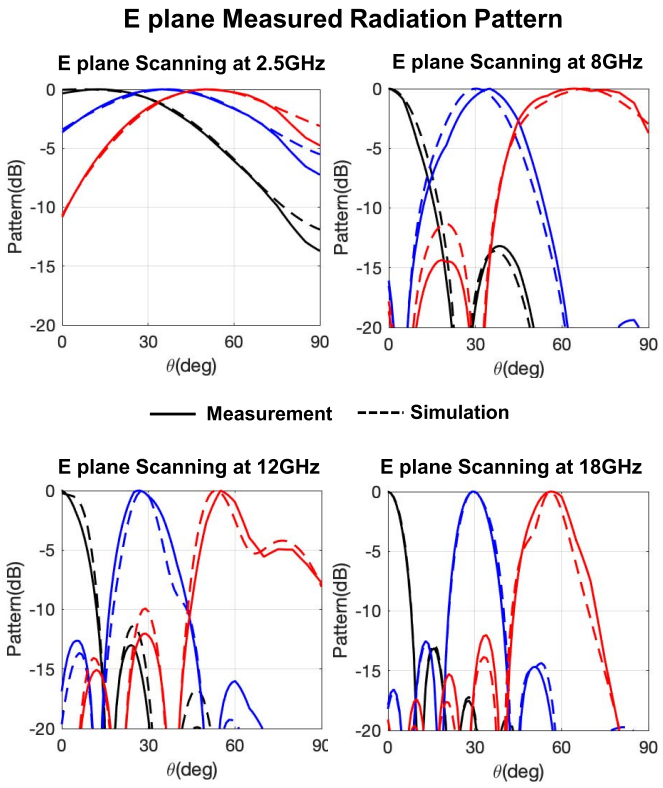

Fig. 11. Measured and simulated normalized radiation pattern in E-plane for 2.5, 8, 12, and 18 GHz. Scanning down to 60°, respectively.

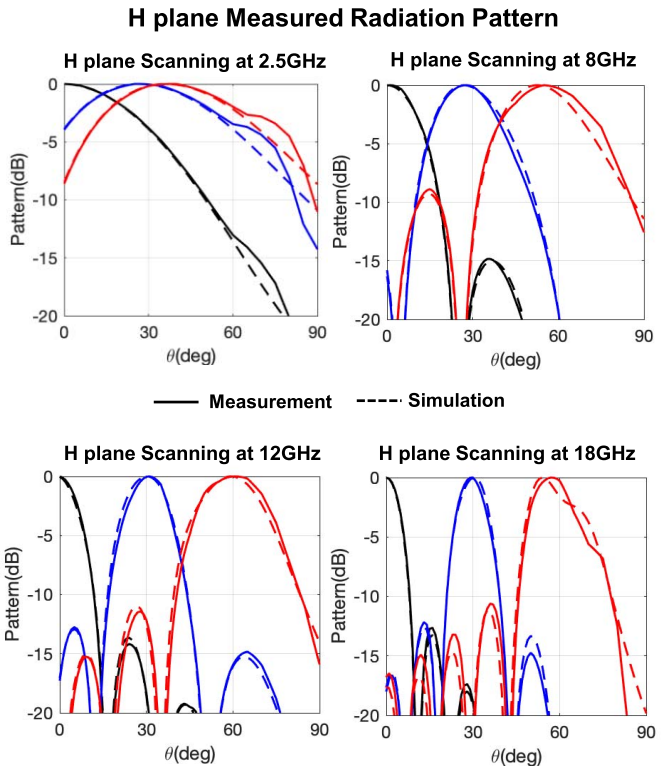

Fig. 12. Measured and simulated normalized radiation pattern in H-plane for 2.5, 8, 12, and 18 GHz. Scanning down to 60°, respectively.

IV. Comparison With Existing Work

As mentioned earlier, the proposed TCDA exhibits the largest ever reported bandwidth of 9:1 without using R-cards in the substrate. Furthermore, although previous TCDAs [10], [11] offered >10:1 bandwidth, they had lower radiation efficiency (even when mismatch losses are excluded). To better assess this improvement from previous designs, we revisit the fundamental bandwidth limit for a conformal array backed by ground plane [19]

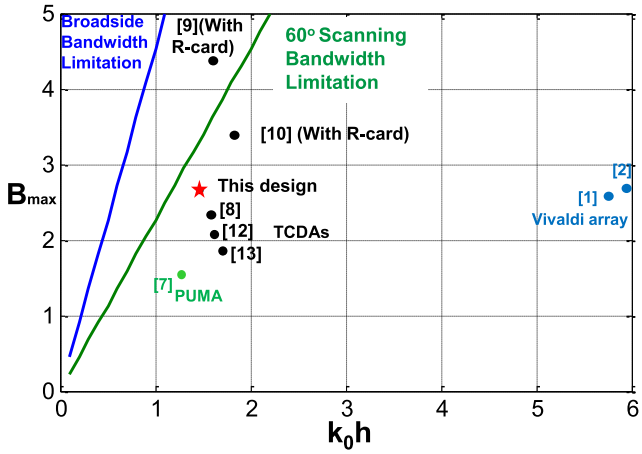

Fig. 13. Bandwidth of different UWB arrays versus their array height, comparing to fundamental bandwidth limit for array over ground plane.

$$B_{max} \leq \frac{\pi \mu_r k_o h cos^p \theta}{log \frac{1}{|\Gamma_{max}|}}. \quad (1)$$

In (1), $B_{\max}$ refers to the maximum achievable bandwidth, k_0 is the free-space wavenumber at the center frequency ω_0, h is the height of the array above the ground plane, θ is the scan angle measured from normal, $\Gamma_{\max}$ is the maximum acceptable reflection coefficient, $p = 1$ refers to the TE polarized wave, and $p = -1$ implies the TM polarized wave.

Using (1), we plot the bandwidth of the presented UWB array in Fig. 13. In Fig. 13, the horizontal axis represents the array height in λ and the vertical axis represents the achievable bandwidth. We remark that the achievable bandwidth depends on the scan angle. In Fig. 13 TCDAs exhibit better bandwidth versus thickness performance as compared with Vivaldi and PUMA arrays. BAVAs are not shown here since there is no data available for 60° scan. The proposed design is labeled with a star in this plot. The TCDA of this paper is closer to the optimal curve as compared with previously reported TCDAs.

V. Concluding Remarks

A new TCDA with integrated feed was presented. The array operates across 2–18 GHz, achieving a 9:1 bandwidth with dual-linear polarization as well as scanning down to 60°. The proposed array is integrated with a folded Marchand balun that also serves as a matching network. To enhance scanning performance, an FSS superstrate is employed to replace traditional dielectric slabs. The developed array exhibits VSWR < 3 at broadside, VSWR < 4 when scanning down to 60° in the E- and D-planes, and down to 30° while scanning into H-plane. In the H-plane, VSWR < 4 across 5–18 GHz. An average total efficiency of 85% is achieved in all cases.

The proposed design was fabricated and measured using a dual-polarized 11 × 11 prototype. The fabricated array was printed on a single three-layer PCB board for low-cost fabrication. The broadside realized gain and radiation patterns were measured and show good agreement with simulations. Measurements also verify scanning down to 60° in the E- and H-planes. In summary, the proposed design

provides a practical solution toward the realization of 2–18 GHz wideband wide-angle scanning phased array.

As for practical applications, we remark that the beamformer is a critical aspect in realizing the potential of this proposed 9:1 UWB array. For such arrays, phase shifters are not practical, and the high-power requirements of ADCs are another challenge for the digital beamforming back-end. To overcome the hardware intensity of the beamformer, the reader is referred to [1], [2], and [20] where a hardware-reduced digital beamformer is proposed. The concept in [1] and [2] encodes the signal right after each antenna. As such many antenna signals can be combined and passed through a fast ADC that serves multiple antenna elements, say 8–16 elements.

REFERENCES

[1] S. B. Venkatakrishnan, D. K. Papantonis, A. A. Akhiyat, E. A. Alwan, and J. L. Volakis, "Experimental validation of on-site coding digital beamformer with ultra-wideband antenna arrays," *IEEE Trans. Microw. Theory Techn.*, vol. 65, no. 11, pp. 4408–4417, Nov. 2017.

[2] S. B. Venkatakrishnan, A. A. Akhiyat, E. A. Alwan, and J. L. Volakis, "Dual-band validation of on-site coding receiver using ultra-wideband antenna array at C, X and Ku-bands," in *Proc. IEEE Antennas Propag. Soc. Int. Symp. (APSURSI)*, Jun. 2016, pp. 1655–1656.

[3] R. W. Kindt and W. R. Pickles, "Ultrawideband all-metal flared-notch array radiator," *IEEE Trans. Antennas Propag.*, vol. 58, no. 11, pp. 3568–3575, Nov. 2010.

[4] J.-B. Yan, S. Gogineni, B. Camps-Raga, and J. Brozena, "A dual-polarized 2–18-GHz Vivaldi array for airborne radar measurements of snow," *IEEE Trans. Antennas Propag.*, vol. 64, no. 2, pp. 781–785, Feb. 2016.

[5] M. W. Elsallal and J. C. Mather, "An ultra-thin, decade (10:1) bandwidth, modular 'BAVA' array with low cross-polarization," in *Proc. IEEE Antennas Propag. Soc. Int. Symp. (APSURSI)*, Jul. 2011, pp. 1980–1983.

[6] H. A. Wheeler, "Simple relations derived fom a phased-array antenna made of an infinite current sheet," *IEEE Trans. Antennas Propag.*, vol. AP-13, no. 4, pp. 506–514, Jul. 1965.

[7] A. Neto and J. J. Lee, "Ultrawide-band properties of long slot arrays," *IEEE Trans. Antennas Propag.*, vol. 54, no. 2, pp. 534–543, Feb. 2006.

[8] S. S. Holland and M. N. Vouvakis, "The planar ultrawideband modular antenna (PUMA) array," *IEEE Trans. Antennas Propag.*, vol. 60, no. 1, pp. 130–140, Jan. 2012.

[9] J. P. Doane, K. Sertel, and J. L. Volakis, "A wideband, wide scanning tightly coupled dipole array with integrated balun (TCDA-IB)," *IEEE Trans. Antennas Propag.*, vol. 61, no. 9, pp. 4538–4548, Sep. 2013.

[10] W. F. Moulder, K. Sertel, and J. L. Volakis, "Ultrawideband superstrate-enhanced substrate-loaded array with integrated feed," *IEEE Trans. Antennas Propag.*, vol. 61, no. 11, pp. 5802–5807, Nov. 2013.

[11] D. K. Papantonis and J. L. Volakis, "Dual-polarized tightly coupled array with substrate loading," *IEEE Antennas Wireless Propag. Lett.*, vol. 15, pp. 325–328, 2015.

[12] M. H. Novak and J. L. Volakis, "Ultrawideband antennas for multiband satellite communications at UHF–Ku frequencies," *IEEE Trans. Antennas Propag.*, vol. 63, no. 4, pp. 1334–1341, Apr. 2015.

[13] E. Yetisir, N. Ghalichechian, and J. L. Volakis, "Ultrawideband array with 70° scanning using FSS superstrate," *IEEE Trans. Antennas Propag.*, vol. 64, no. 10, pp. 4256–4265, Oct. 2016.

[14] M. H. Novak, F. A. Miranda, and J. L. Volakis, "Ultra-wideband phased array for small satellite communications," *IET Microw., Antennas Propag.*, vol. 11, no. 9, pp. 1234–1240, Jul. 2017.

[15] J. Zhong, E. A. Alwan, and J. L. Volakis, "7.2 to 1 ultra-wideband dual-linear polarized phased array with 60° scanning," in *Proc. IEEE Antennas Propag. Soc. Int. Symp. (APSURSI)*, Jul. 2017, pp. 1893–1894.

[16] J. Zhong, E. A. Alwan, and J. L. Volakis, "Ultra-wideband dual-linear polarized phased array with 60° scanning for simultaneous transmit and receive systems," in *Proc. Int. Workshop Antenna Technol., Small Antennas, Innov. Struct., Appl. (iWAT)*, Mar. 2017, pp. 140–141.

[17] D. M. Pozar, "The active element pattern," *IEEE Trans. Antennas Propag.*, vol. 42, no. 8, pp. 1176–1178, Sep. 1994.

[18] A. Ludwig, "The definition of cross polarization," *IEEE Trans. Antennas Propag.*, vol. AP-21, no. 1, pp. 116–119, Jan. 1973.

[19] J. P. Doane, K. Sertel, and J. L. Volakis, "Matching bandwidth limits for arrays backed by a conducting ground plane," *IEEE Trans. Antennas Propag.*, vol. 61, no. 5, pp. 2511–2518, May 2013.

[20] S. B. Venkatakrishnan, A. Akhiyat, E. A. Alwan, and J. L. Volakis, "Multiband and multibeam direction of arrival estimation using on-site coding digital beamformer," *IEEE Antennas Wireless Propag. Lett.*, vol. 16, pp. 2332–2335, 2017.